Computational and Structural Biotechnology Journal 23 (2024) 2938–2948

Contents lists available at ScienceDirect

Computational and Structural Biotechnology Journal

journal homepage: www.elsevier.com/locate/csbj

Research Article

Strengths and limitations of web servers for the modeling of TCRpMHC complexes

Hoa Nhu Le, Martiela Vaz de Freitas, Dinler Amaral Antunes *

University of Houston, Departments of Biology and Biochemistry, Houston, 77204, TX, USA

ARTICLE INFO

Keywords:
T-cell
TCRpMHC
TCRpMHCmodels
AlphaFold
ImmuneScape
TCRmodel2

ABSTRACT

Cellular immunity relies on the ability of a T-cell receptor (TCR) to recognize a peptide (p) presented by a class I major histocompatibility complex (MHC) receptor on the surface of a cell. The TCR-peptide-MHC (TCRpMHC) interaction is a crucial step in activating T-cells, and the structural characteristics of these molecules play a significant role in determining the specificity and affinity of this interaction. Hence, obtaining 3D structures of TCRpMHC complexes offers valuable insights into various aspects of cellular immunity and can facilitate the development of T-cell-based immunotherapies. Here, we aimed to compare three popular web servers for modeling the structures of TCRpMHC complexes, namely ImmuneScape (IS), TCRpMHCmodels, and TCRmodel2, to examine their strengths and limitations. Each method employs a different modeling strategy, including docking, homology modeling, and deep learning. The accuracy of each method was evaluated by reproducing the 3D structures of a dataset of 87 TCRpMHC complexes with experimentally determined crystal structures available on the Protein Data Bank (PDB). All selected structures were limited to human MHC alleles, presenting a diverse set of peptide ligands. A detailed analysis of produced models was conducted using multiple metrics, including Root Mean Square Deviation (RMSD) and standardized assessments from CAPRI and DockQ. Special attention was given to the complementarity-determining region (CDR) loops of the TCRs and to the peptide ligands, which define most of the unique features and specificity of a given TCRpMHC interaction. Our study provides an optimistic view of the current state-of-the-art for TCRpMHC modeling but highlights some remaining challenges that must be addressed in order to support the future application of these tools for TCR engineering and computer-aided design of TCR-based immunotherapies.

1. Introduction

T-cell lymphocytes play a crucial role in the immunosurveillance against cellular diseases, including cancer and infections by intracellular pathogens [1,2]. Central to this function is the ability to specifically recognize diseased cells that must be eliminated, while avoiding harm to healthy cells. $CD8^+$ cytotoxic T cells are known for their remarkable specificity, which is made possible by the expression of unique T-cell receptors (TCRs). These receptors recognize peptide-targets derived from intracellular proteins, which are presented on the cell surface via class I Major Histocompatibility Complex (MHC-I) receptors (Fig. 1). The MHC-I binding cleft encloses both ends of the peptide, having deeper pockets that accommodate specific "anchor" residues in the peptide ligands (e.g., pockets B and F) [3,4]. Note that MHC-I receptors are encoded by the most polymorphic genes in the human genome, and different MHC alleles encode different pockets, in turn leading to different requirements for peptide binding [5]. Adding to that diversity, the pool of displayed peptides reflects both the genetic diversity of the host (i.e., the proteome of a healthy cell) and that of the pathogen or cancer (e.g., viral proteins or cancer neoantigens) [1]. Therefore, peptide-MHC (pMHC) complexes loaded with peptides derived from tumoral or viral proteins can serve as molecular targets for TCR recognition. However, recognition of these diverse pMHC targets requires elaborated mechanisms to promote the diversity of TCR specificities, which are reflected in the unique structural features of individual TCR molecules [6].

TCRs are heterodimers usually consisting of one α and one β chain [7], each one composed of a constant and a variable region [8,9]. The variable regions of each chain include three highly variable complementarity-determining region (CDR) loops, of which the most diverse is the CDR3β (i.e., unique sequences and structures, as determined by the somatic rearrangement of V(D)J gene segments). Together, the combined surface of the 6 CDR loops forms the TCR interface that specif-

* Corresponding author.
E-mail address: dinler@uh.edu (D.A. Antunes).

https://doi.org/10.1016/j.csbj.2024.06.028
Received 31 March 2024; Received in revised form 22 June 2024; Accepted 23 June 2024
Available online 1 July 2024

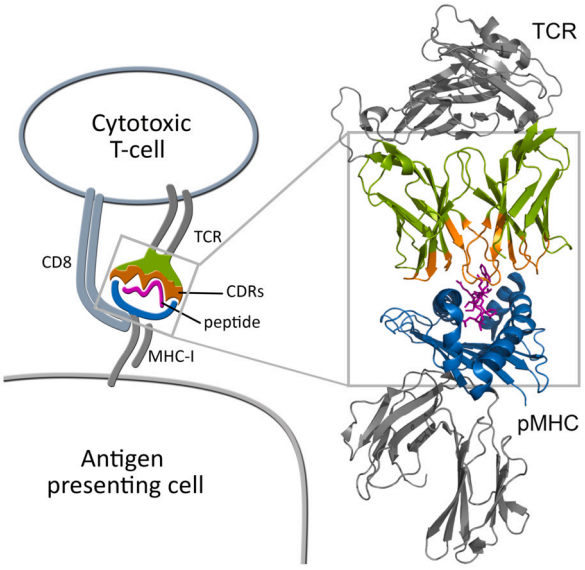

Fig. 1. The TCRpMHC structure. A. On the left, schematic view of a $CD8^+$ lymphocyte using the T-cell receptor (TCR) to recognize a peptide-loaded class I Major Histocompatibility Complex (pMHC) at the surface of an antigen-presenting cell (APC). The interaction is further stabilized by the CD8 glycoprotein. The extracellular portion of the TCRpMHC structure is presented on the right side (*cartoon*). The grey box indicates the cropped structure that was used for all analyses in this study, limited to the $\alpha 1$ and $\alpha 2$ domains of the MHC receptor (blue), the peptide ligand (purple), and the variable TCR domains ($V\alpha/V\beta$, in green), which include the Complementarity Determining Region (CDR) loops (orange). B. Surface representation of the same cropped structure. Separation between TCR (shades of green) and pMHC (purple/blue) was increased for visualization purposes. C. Representation of the Crossing Angle, capturing the TCR twist motion. D. Representation of the Incident Angle, capturing the TCR tilt motion.

ically interacts with a cognate pMHC complex (Fig. 1). It is important to note, however, that the same TCR can engage with multiple pMHC complexes, a phenomenon known as T-cell cross-reactivity [10,9,11,1]. This feature of cellular immunity enables a limited pool of T-cells to provide broader coverage against a more comprehensive range of targets [12]. On the other hand, T-cell cross-reactivity can lead to autoimmune reactions and off-target toxicity, representing a significant safety concern for T-cell-based immunotherapies [1,13]. In this context, understanding the molecular and structural features driving the specificity of TCRpMHC interactions is central to the development of better and safer T-cell-based immunotherapies, particularly those involving TCR engineering efforts (e.g., TCR-T and TCR-mimic CAR-T cell therapies) [14–17].

In recent decades, much has been learned from TCRpMHC structures determined with experimental assays [8,18,4,19,20], such as X-ray crystallography, but the cost and time required to resolve a single structure prevent the use of these approaches for large-scale analysis. On the other hand, the aforementioned diversity of TCRpMHC complexes requires the detailed structural analysis of potentially millions of TCRpMHC complexes to identify therapeutic opportunities, particularly for personalized immunotherapies. As a consequence, there is growing interest in the development of accurate and scalable computational methods for the structural modeling of TCRpMHC complexes, which is becoming a crucial step for the development of novel T-cell-based immunotherapies [21–23]. However, the limited experimental data available for training and the extreme variability of the TCRpMHC molecules, including diverse docking orientations (Fig. 1), all contribute to making this a very challenging problem in computational biology [23].

In this work, we evaluate the accuracy of available web servers for the structural prediction of TCRpMHC complexes. The selected web servers have efficient implementations but rely on distinct computational approaches, including molecular docking, homology modeling, and deep learning. We analyzed the strengths and limitations of these

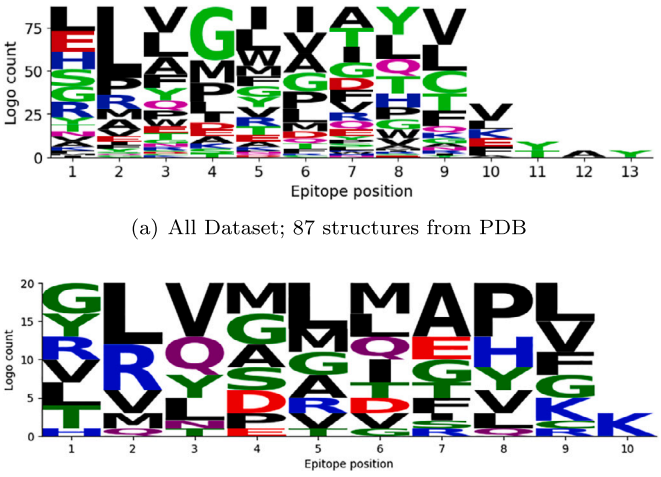

(a) All Dataset; 87 structures from PDB

(b) New Dataset; 20 structures after 2021

Fig. 2. Sequence logo of peptides from studied complexes. The logo plot illustrates the distribution and prevalence of amino acids by position across all 87 peptide sequences (a) or a subset of 20 peptides from structures published after 2021 (b). The All dataset includes one 8-mer, 55 9-mer, 22 10-mer, five 11-mer, and four 13-mer. There is no dominant sequence motif in the All dataset, aside from a preference for Leucine in p2, which is compatible with HLA-A2 supertype binding preference.

methods by reproducing a reference dataset of 87 experimentally determined TCRpMHC structures. We assessed the accuracy of the produced models using an assortment of metrics capturing both the geometry of the individual molecules and how they interact as a complex (e.g., intermolecular contacts and docking orientation).

2. Method

2.1. Data preparation

Our dataset consists of 87 TCRpMHC complexes with (i) structures determined experimentally and available at the Protein Data Bank (PDB) [24], and (ii) curated annotations at the Immune Epitope Database (IEDB) [25]. All these structures were determined by X-ray crystallography, having average, min, and max resolution of 2.57 Å, 1.54 Å and 3.51 Å, respectively (Table 1).

These complexes cover a diversity of peptide ligand sources, including 39 viral, 28 cancer-associated, 13 “self” (human), 4 synthetic, and 3 bacterial peptides. The peptide sequences were also very diverse (Fig. 2(a)), with the exception of peptide anchor position 2 (p2). This position exhibited a noticeable preference for leucine (L), a bias that is consistent with the overrepresentation of the HLA-A2 supertype in the dataset. In addition to HLA-A2, our dataset also includes HLA-A24-restricted structures, as well as structures with HLA-B and HLA-C alleles (Table 1).

The FASTA sequences and crystal structures of selected complexes were downloaded from the PDB. All structures were manually truncated to reduce the overall size of the modeled complexes (Fig. 1), which in turn reduces the required computing time and increases the precision of all analyses. Specifically, only the variable domains of the TCR chains were retained, removing the constant regions that are not part of the binding site. On the MHC, only the α-1 and α-2 domains were retained for further analysis, therefore removing the α-3 domain and the β2-microglobulin.

2.2. Modeling protocols

We used three different web servers to predict TCRpMHC complexes based on various approaches: namely TCRpMHCmodels [26],

Table 1
A comprehensive table of TCR-Peptide-HLA complexes.

#	PDB ID	Epitope	Source	Allele	TCR ID	Method	Resolution
Structures generated prior 2021							
1	1AO7	LLFGYPVYV	virus	HLA-A*02:01	AV2S1A2, BV13S1	X-ray diffraction	2.6
2	1BD2	LLFGYPVYV	virus	HLA-A*02:01	ADV21S1A1N2, BV13S1	X-ray diffraction	2.5
3	1MI5	FLRGRAYGL	virus	HLA-B*08:01	TRAC, TRAB	X-ray diffraction	2.5
4	1QRN	LLFGYAVYV	virus	HLA-A*02	TRAC, TRAB	X-ray diffraction	2.8
5	1QSF	LLFGYPVAV	virus	HLA-A*02	TRAC, TRAB	X-ray diffraction	2.8
6	2AK4	LPEPLPQGQLTAY	virus	HLA-B*35:08	SB27	X-ray diffraction	2.5
7	2BNQ	SLLMWITQV	synthetic	HLA-A*02	TRAC, TRAB	X-ray diffraction	1.7
8	2BNR	SLLMWITQC	synthetic	HLA-A*02	TRAC, TRAB	X-ray diffraction	1.9
9	2F53	SLLMWITQC	cancer	HLA-A*02:01	TRAC, TRAB	X-ray diffraction	2.1
10	2F54	SLLMWITQC	cancer	HLA-A*02:01	TRAC, TRAB	X-ray diffraction	2.7
11	2P5E	SLLMWITQC	cancer	HLA-A*02	TRAC, hypothetical protein	X-ray diffraction	1.89
12	2P5W	SLLMWITQC	cancer	HLA-A*02	TRAC, hypothetical protein	X-ray diffraction	2.2
13	2VLJ	GILGFVFTL	virus	HLA-A*02:01	JM22	X-ray diffraction	2.4
14	2VLR	GILGFVFTL	virus	HLA-A*02:01	JM22	X-ray diffraction	2.3
15	3DXA	EENLLDFVRF	virus	HLA-B*44:05	DM1	X-ray diffraction	3.5
16	3FFC	FLRGRAYGL	synthetic	HLA-B*08	CF34	X-ray diffraction	2.8
17	3GSN	NLVPMVATV	virus	HLA-A*02	TRAV24, TRBV6-5	X-ray diffraction	2.8
18	3H9S	MLWGYLQYV	self	HLA-A*02	A6 TRAC, TRBV6-5	X-ray diffraction	2.7
19	3HG1	ELAGIGILTV	cancer	HLA-A*02:01	TRAC, TRAB	X-ray diffraction	3
20	3KPR	EEYLKAWTF	virus	HLA-B*44:05	LC13	X-ray diffraction	2.6
21	3KPS	EEYLQAFTY	self	HLA-B*44:05	LC13	X-ray diffraction	2.7
22	3KXF	LPEPLPQGQLTAY	virus	HLA-B*35:08	SB27	X-ray diffraction	3.1
23	3MV7	HPVGEADYFEY	virus	HLA-B*35:01	TK3	X-ray diffraction	2
24	3MV8	HPVGEADYFEY	virus	HLA-B*35:01	TK3	X-ray diffraction	2.1
25	3MV9	HPVGEADYFEY	virus	HLA-B*35:01	TK3	X-ray diffraction	2.7
26	3O4L	GLCTLVAML	virus	HLA-A*02:01	TRAC, TRAB	X-ray diffraction	2.54
27	3PWP	LGYGFVNYI	self	HLA-A*02:01	A6	X-ray diffraction	2.69
28	3QDG	ELAGIGILTV	cancer	HLA-A*02:01	DMF5	X-ray diffraction	2.69
29	3QDJ	AAGIGILTV	cancer	HLA-A*02	DMF5	X-ray diffraction	2.3
30	3QDM	ELAGIGILTV	cancer	HLA-A*02	DMF4	X-ray diffraction	2.8
31	3QEQ	AAGIGILTV	cancer	HLA-A*02	DMF4	X-ray diffraction	2.59
32	3QFJ	LLFGFPVYV	virus	HLA-A*02	A6	X-ray diffraction	2.29
33	3UTT	ALWGPDPAAA	self	HLA-A*02:01	1E6	X-ray diffraction	2.6
34	3VXM	RFPLTFGWCF	virus	HLA-A*024	C1-28	X-ray diffraction	2.5
35	3VXR	RYPLTFGWCF	virus	HLA-A*024	H27-14	X-ray diffraction	2.4
36	3VXS	RYPLTLGWCF	virus	HLA-A*024	H27-14	X-ray diffraction	1.8
37	3VXU	RFPLTFGWCF	virus	HLA-A*24	T36-5	X-ray diffraction	2.7
38	4FTV	LLFGYPVYV	virus	HLA-A*02	A6	X-ray diffraction	2.74
39	4G8G	KRWIILGLNK	virus	HLA-B*27:05	C12C	X-ray diffraction	2.4
40	4G9F	KRWIIMGLNK	virus	HLA-B*27:05	C12C	X-ray diffraction	1.9
41	4JFD	ELAAIGILTV	cancer	HLA-A*02	high affinity TCRA, TCRB	X-ray diffraction	2.46
42	4JFE	ELAGIGALTV	cancer	HLA-A*02:01	high affinity TCRA, TCRB	X-ray diffraction	2.7
43	4JFF	ELAGIGILTV	cancer	HLA-A*02	high affinity TCRA, TCRB	X-ray diffraction	2.43
44	4JRX	LPEPLPQGQLTAY	virus	HLA-B*35:05	CA5	X-ray diffraction	2.3
45	4JRY	LPEPLPQGQLTAY	virus	HLA-B*35:05	SB47	X-ray diffraction	2.8
46	4L3E	ELAGIGILTV	cancer	HLA-A*02:01	DMF5	X-ray diffraction	2.56
47	4MJI	TAFTIPSI	virus	HLA-B*51:01	TRAC, TRAB	X-ray diffraction	2.99
48	4MNQ	ILAKFLHWL	self	HLA-A*02:01	LOC452776, TRBC1	X-ray diffraction	2.74
49	4PRH	HPVGDADYFEY	virus	HLA-B*35:08	TK3	X-ray diffraction	2.5
50	4PRI	HPVGEADYFEY	virus	HLA-B*35:08	TK3	X-ray diffraction	2.4
51	4QOK	EAAGIGILTV	cancer	HLA-A*02	Mel5	X-ray diffraction	3
52	4QRP	HSKKKCDEL	virus	HLA-B*08:01	DD31	X-ray diffraction	2.9
53	5D2L	NLVPMVATV	virus	HLA-A*02	C7	X-ray diffraction	3.51
54	5D2N	NLVPMVATV	virus	HLA-A*02	C25	X-ray diffraction	2.1
55	6Q3S	SLLMWITQV	synthetic	HLA-A*02:01	TRAV21, TRBV6-5	X-ray diffraction	2.5
56	6R2L	SLSKILDTV	cancer	HLA-A*02:01	TRAV22, TRBV11-2	X-ray diffraction	2.3
57	6RP9	SLLMWITQV	cancer	HLA-A*02:01	NYE_S1	X-ray diffraction	3.12
58	6RPB	SLLMWITQV	cancer	HLA-A*02:01	NYE_S3	X-ray diffraction	2.5
59	6RSY	RMFPNAPYL	cancer	HLA-A*02:01	A7B2	X-ray diffraction	2.95
60	6TMO	EAAGIGILTV	cancer	HLA-A*02:01	A24B17	X-ray diffraction	2.1
61	6TRO	GVYDGREHTV	cancer	HLA-A*02:01	GVY01	X-ray diffraction	3
62	6UON	GADGVGKSAL	cancer	HLA-A*02:01	GVY01	X-ray diffraction	3.5
63	6VMX	RPPIFIRRL	virus	HLA-B*07:02	HD14	X-ray diffraction	3.1
64	6VQO	HMTEVVRHC	cancer	HLA-A*02:01	1A2	X-ray diffraction	3
65	6VRM	HMTEVVRHC	cancer	HLA-A*02:01	12-6	X-ray diffraction	2.61
66	6VRN	HMTEVVRHC	cancer	HLA-A*02:01	38-10	X-ray diffraction	2.61
67	7N6E	YLQPRTFLL	virus	HLA-A*02:01	NR1C	X-ray diffraction	3.2

(*continued on next page*)

Table 1 (*continued*)

#	PDB ID	Epitope	Source	Allele	TCR ID	Method	Resolution
Structures generated after 2021							
68	7N1E	RLQSLQTYV	virus	HLA-A*02:01	RLQ3	X-ray diffraction	2.3
69	7N1F	YLQPRTFLL	virus	HLA-A*02:01	pYLQ7	X-ray diffraction	2.39
70	7N2N	TRLALIAPK	self	HLA-B*27:05	AS4.2	X-ray diffraction	2.6
71	7N2O	LRVMMLAPF	bacteria	HLA-B*27:05	AS4.2	X-ray diffraction	2.3
72	7N2P	GQVMVVAPR	self	HLA-B*27:05	AS4.3	X-ray diffraction	2.5
73	7N2Q	LRVMMLAPF	bacteria	HLA-B*27:05	AS4.3	X-ray diffraction	2.7
74	7N2R	TRLALIAPK	self	HLA-B*27:05	AS4.3	X-ray diffraction	2.28
75	7N2S	TRLALIAPK	self	HLA-B*27:05	AS3.1	X-ray diffraction	2.37
76	7OW5	VVVGAGGVGK	self	HLA-A*11:01	JDIa41b1	X-ray diffraction	2.58
77	7OW6	VVVGADGVGK	self	HLA-A*11:01	JDIa41b1	X-ray diffraction	2.64
78	7PB2	VVVGADGVGK	self	HLA-A*11:01	JDI	X-ray diffraction	3.41
79	7PBC	GLYDGMEHL	cancer	HLA-A*02:01	c796	X-ray diffraction	2.04
80	7PBE	YLQPRTFLL	virus	HLA-A*02:01	YLQ36	X-ray diffraction	3
81	7PDW	GLYDGMEHL	cancer	HLA-A*02:01	c728	X-ray diffraction	1.82
82	7QPJ	GLYDGMEHL	cancer	HLA-A*02:01	c756	X-ray diffraction	1.54
83	7RK7	YMNGTMSQV	self	HLA-A*02:01	TIL1383I	X-ray diffraction	2.54
84	7RM4	HMTEVVRHC	cancer	HLA-A*02:01	6-11	X-ray diffraction	3.33
85	8CX4	LRVMMLAPF	bacteria	HLA-B*27:05	AS8.4	X-ray diffraction	2.2
86	8GOM	RLQSLQTYV	virus	HLA-A*02:01	RLQ7	X-ray diffraction	2.78
87	8GON	RLQSLQIYV	virus	HLA-A*02:01	RLQ7	X-ray diffraction	2.6

ImmuneScape (IS) [27] and TCRmodel2 [2]. TCRmodel2, the newest method, is a tailored implementation of AlphaFold2 (AF2) [28]. Hence, we also included AF2 in our analysis to provide baseline performance for a general-purpose deep-learning method.

TCRpMHCmodels [26] is a publicly available web server that uses the amino acid sequences of MHC α chain, peptide chain, and TCR α and β chains as input to predict the 3D structure of TCRpMHC complexes. This tool can be accessed on the DTU Health Tech bioinformatics services webpage. TCRpMHCmodels rely on homology modeling with MODELLER v9.18 automodel class and default settings [26], with the modeling of each complex taking approximately 5 minutes. To support that, three separate template databases are used to model the pMHC, TCR, and TCRpMHC complexes, respectively. The pMHC template database encompasses 455 pMHC structures sourced from IEDB and PDB. A Hidden Markov Model uses these datasets to construct a comprehensive profile for MHC class I, drawing from all the sequences in the database. The TCR template database has 105 paired TCR chains curated from LYRA [29]. Finally, the TCRpMHC template database is comprised of 61 structures obtained from IEDB and PDB.

ImmuneScape (IS) also uses amino acid sequences as input to predict TCRpMHC structures, but this tool's protocol is centered on molecular docking [27]. This tool is directly accessible from the Systems Immunology lab's webpage. Unlike the TCRpMHCmodels tool, the user can select the MHC alleles by name without having to provide a sequence. The modeling also takes around 5 minutes per model and encompasses six main steps. First, TCR chains are modeled with LYRA and Repertoire Builder. Second, NetMHCpan and BLOSUM62 are used to choose the pMHC template. Next, the BLOSUM62 matrix implemented in MAFFT [30] selects the docking template. Then, TCR chains are docked into the docking template using conserved residues as anchor positions, followed by pMHC side chain remodeling with SCWRL4 [31]. Lastly, different models are ranked with BLAST, Repertoire Builder scores, and EMPIRE score [27], a TCR-pMHC binding energy function.

The TCRmodel2 tool is a web server developed by the Pierce Lab at the University of Maryland Institute for Bioscience and Biotechnology Research. It leverages the recent development of AF2 and includes several modifications across the AF2 pipeline to improve the prediction for TCRpMHC complexes. First, the multiple sequence alignment (MSA) is modified to use an extensive database with all structures of TCRs and MHCs up to 2021. Next, TCRmodel2 searches for templates in PDB using only the TCR sequences rather than the entire MSA. Afterward, pMHC templates are selected from PDB, and customized template features are used. Finally, all models are scored with AF2 scoring functions, including the average predicted local difference distance test and the predicted templates score [2]. The inputs are the same as those in TCRpMHCmodels, and the modeling takes around 20 minutes per complex.

Unlike the aforementioned methods, AF2 [28] was initially developed as a general method for the structural prediction of monomeric proteins. Its methodology uses the most advanced deep learning algorithms and heavily relies on information from the MSA. The MSA is used to identify correlations between residue positions that might contact each other in 3D space and select templates from the PDB. Their pipeline contains three modules. First is the input module, where AF2 searches for homologous sequences in the database to collect information on MSA and pairwise distance matrix. To this end, AF2 implemented several search tools, including JackHMMer, HHBlits, and HHsearch. The second module is called Evoformer, in which the output of the previous module is used to create MSA representation and pair representation. The last is the structure module, in which pair representation and backbone frames are used to predict relative rotations and translations, leading to the prediction of angles and atoms' positions, finally producing and ranking multiple structural models [28,32]. The modeling lasted more than 2 hours per complex.

2.3. Model processing and accuracy assessment

The numbering of atoms and amino acids is often inconsistent between the reference crystal structures and the models produced by different tools. Therefore, to prevent errors in subsequent analysis, the sequences of produced models were corrected as needed with the BioPython package (Fig. 3). First, the sample model was compared to a reference structure to identify differences in chain IDs, chain order, residue indices, and missing residues. If a mismatch was observed, the function PairwiseAligner was used to score the pairwise similarity between them. Based on the scores, we could relabel the chains of the sample structure according to those of the reference structure. In the case of crystal structures, heteroatoms, and water residues were also removed. Lastly, we fixed the residue indices in the target structure. Here, we used IS models as a reference for indexing.

For an initial overall assessment of model quality, we employed the normalized discrete optimized protein energy (DOPE) method [33], which was used to compute Z-scores. Subsequently, we utilized the nclash value from the CAPRI assessment [34] to determine the presence of clashes in the models (e.g., values higher than 1 indicate clashes).

To further evaluate model accuracy, we calculated the root mean square deviation (RMSD) values between models and crystal structures for five different groups of atoms: (i) all proteins, (ii) MHC, (iii) peptide,

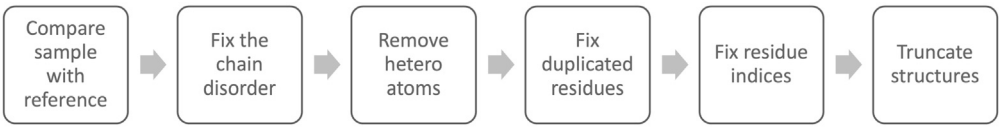

Fig. 3. The process for correcting the residue labeling of TCRpMHC, TCRmodel2 models, and crystal structures. Models were first compared with reference to fix the chain order. Next, we removed the heteroatoms and fixed any duplicated residues and residue indices to ensure all models from the same structure had the same number of atoms.

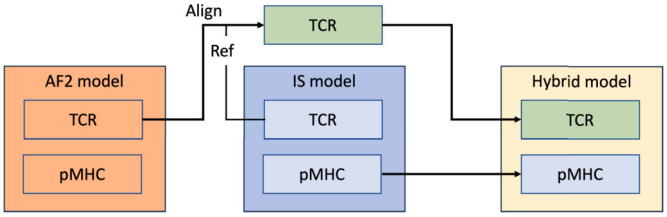

Fig. 4. The hybrid modeling approach. First, AF2 models were aligned with the corresponding IS models (Reference). Then, the aligned TCR from AF2 and the pMHC from the IS are combined to create the hybrid model for each TCRpMHC complex.

(iv) TCR, and (v) CDR loops. These RMSD were calculated for Cα atoms, using the class Superimposed in BioPython.

Additionally, we used four other metrics to evaluate different aspects of model accuracy. First, the CAPRI assessment involves the analysis of several critical parameters to evaluate the quality of a protein-ligand complex model. It includes the fnat and fnon-nat, which represent the fraction of receptor-ligand residue contacts in the model that are accurately reproduced in the target structure and the fraction of contacts in the model that are not present in the target, respectively. Additionally, the root-mean-square (rms) displacement of the backbone atoms of the ligand (L-rms), as well as the misorientation angle (uL) and residual displacement (dL) of the ligand are used to determine the global geometry of the model. Furthermore, the rms of interface backbone (I-rms) and interface side-chain (S-rms) atoms are computed after superimposing the interface residues [35]. Second, the DockQ combines key parameters of the CAPRI assessment (i.e., fnat, L-rms and I-rms) into a unified scoring system within the interval of 0 to 1. Finally, the TCR crossing angle and incident angle, as defined by TCR3d [36], were calculated with the TCR3d website and used to analyze the TCR orientation in all models. The crossing angle captures the "TCR twist" in relation to the pMHC. It is calculated by the angle formed between the plane separating the TCR domains and that of the MHC's peptide-binding cleft (Fig. 1(c)). The incident angle captures the "TCR tilt" in relation to the pMHC. It is calculated by the angle between the normal vector of the MHC's peptide-binding cleft plane and the TCR interdomain axis of rotation (Fig. 1(d)).

In order to better explore our results and investigate the differences between the tailored protocol of TCRmodel2 and the baseline protocol of AF2, we also implemented a hybrid methodology combining steps from AF2 and IS (Fig. 4). In this protocol, the TCR chains from an AF2 model are aligned with the TCR chains in a corresponding IS model. Afterward, the TCR chain from IS is removed, and the hybrid TCRpMHC structure is saved to a PDB file for subsequent analysis.

2.4. Statistical analysis

We conducted a Tukey's Honestly Significant Difference (HSD) test to pairwise compare the means of Root Mean Square Deviation (RMSD) across multiple methods. In this post hoc test, the null hypothesis is that the RMSD distributions underlying the methods all have the same mean, while the alternative hypothesis is that their means are different. Then, p-values and confidence intervals for mean differences were obtained with the `tukey_hsd` function in the Scipy.stats package [37]. The same statistical test was also used to assess the distributions of crossing angles and incident angles of structures.

2.5. Computational resources

Modeling with TCRmodel2, TCRpMHCmodels, and IS was conducted in their respective web servers, as described in section 2.2. The AF2 models were run on a high-performance computing (HPC) cluster at the University of Houston's Research Computing Data Core (RCDC). Each computational run utilized 32 cores or two full nodes, with 3750 MB memory per CPU and 3 GPUs. The average run time for each execution was approximately two hours.

3. Results and discussion

3.1. Dedicated web servers outperform AlphaFold2 in TCRpMHC modeling

In this study, a dataset consisting of 87 TCRpMHC complexes (Table 1) was employed to compare the predictive performance of four modeling approaches: AF2, IS, TCRmodel2, and TCRpMHCmodels. We first evaluated the quality of models by using the normalized DOPE z-score method and the nclash value from the CAPRI assessment. Models with positive Z-scores are anticipated to be inaccurate, while those with Z-scores below -1 are deemed more native-like. It's noteworthy that none of our models yielded positive Z-scores. Nevertheless, we identified several models with Z-scores equal to or greater than -1, including three IS models, one AF2 model, two hybrid models, one TCRmodel2, and 47 TCRpMHCmodels. Besides, the CAPRI results revealed that multiple models contained clashes, including 7 IS models, one AF2 model, and 38 hybrid models.

In the initial phase of our analysis, we conducted an assessment of the root mean square deviation (RMSD) average across the entire TCRpMHC complex (e.g., "all protein" atom selection). This analysis provides a coarse evaluation of the overall accuracy of the modeled TCRpMHC complexes, considering both chain conformations and TCR docking orientation. In this comparison, IS had the lowest Cα RMSD average (2 Å), followed by TCRpMHCmodels (2.4 Å) and TCRmodel2 (2.6 Å). However, the differences between these averages were not statistically significant. In contrast, all three dedicated methods performed significantly better than the general purpose AF2 implementation (7.3 Å) (Fig. 5(a)).

To focus on the most challenging components of the system, we divided the TCRpMHC complexes into smaller groups of atoms and repeated the RMSD calculations. Again, the three dedicated web servers performed approximately equally across predicting the MHC, peptide, TCR, and CDR loops. As expected, AF2 generated good models for the highly conserved MHC structures (average Cα RMSD of 0.8 Å) but failed to predict the peptide-ligand conformations (average Cα RMSD of 5 Å). Note that modeling MHC-bound peptide conformations remains a persistent challenge in the field [3,38], especially for non-template-based methods such as AF2 [28,39]. This is due to the fact that the peptide structure is determined mainly by the MHC cleft and not by the peptide sequences [3,40]. It is important to note that AF2-derived MHC predictions were still statistically higher than those of dedicated methods, according to the ANOVA with Tukey post-hoc test. Surprisingly, AF2 models showed no significant difference in Cα RMSD compared to other methods while predicting TCRs and the highly variable CDR loops (Fig. 5(d), 5(e)).

These results also showed that TCRmodel2 did a remarkably better job than the general purpose AF2 in predicting TCRpMHC complexes

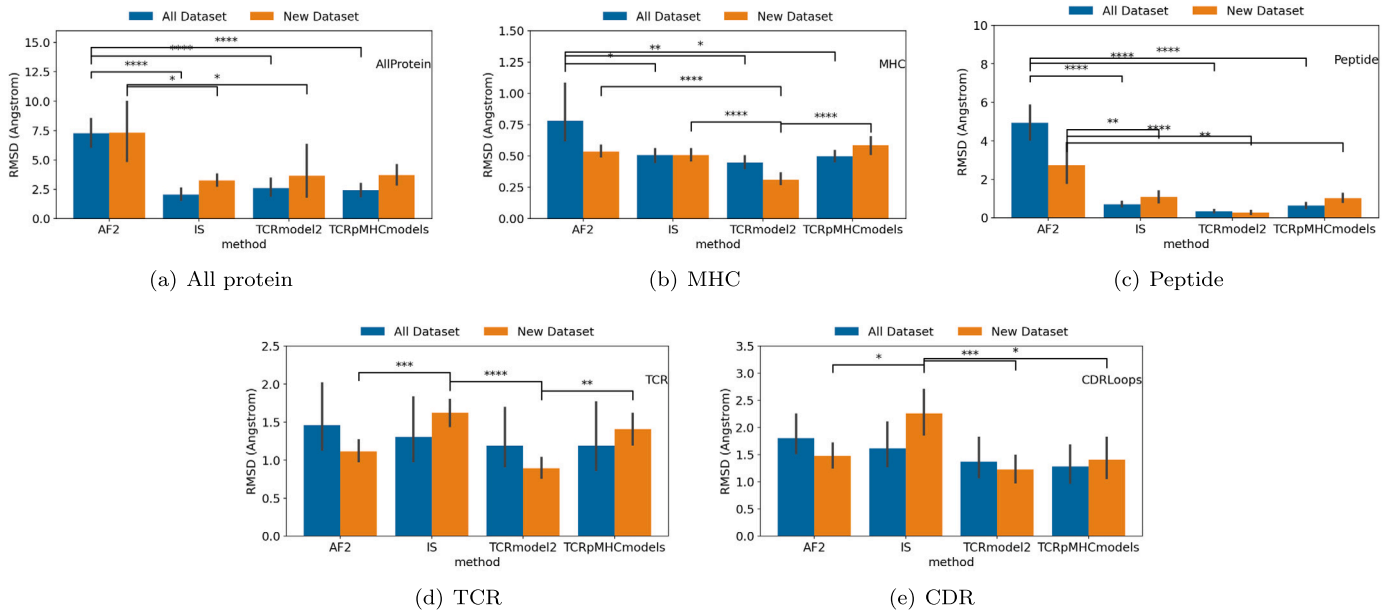

(a) All protein (b) MHC (c) Peptide

(d) TCR (e) CDR

Fig. 5. Carbon alpha root mean square deviation (Cα RMSD) between models and reference crystal structures, computed for 87 TCRpMHC structures ("All dataset"). Models were produced using four methods: IS, TCRpMHCmodels, TCRmodel2, and AF2. The average Cα RMSD values were computed from different groups of atoms: (a) all protein, (b) MHC, (c) peptide, (d) TCR, and (e) CDR loops.

(Fig. 5). In addition, TCRmodel2 produced functional models for all 87 targeted complexes, while some issues were observed with the other methods. For instance, TCRpMHCmodels failed to generate a model for five complexes without providing additional information. And IS generated models for all 87 complexes, but 12 of the models had clashes or structural issues that would require further refinement. In two of the most concerning cases, a CDR loop was modeled in a way that its backbone was looping around a segment of the MHC or the peptide.

Surprisingly, no statistical difference was observed between TCRmodel2 and the different methods (IS and TCRpMHCmodels) regarding the RMSD values across the atom groups tested. This is despite TCRmodel2 leveraging the deep learning algorithms of AF2 and having been trained in a much larger (more recent) dataset of templates. TCRmodel2 uses all TCRpMHC crystal structures published up to 2021, while the other methods used data before 2020 [27,26].

3.2. TCR docking orientation remains a significant challenge

Since our reference dataset overlapped with the datasets used to develop these modeling tools, we decided to evaluate the extent to which this overlap could be biasing the results. To do that, we repeated our analysis in a subset of 20 structures published after 2021 (Table 1). Given their publication date, these structures have never been "seen" by the three modeling methods. This analysis confirmed the bias in favor of the dedicated web servers, reducing the gap in relation to AF2 results. The most significant performance reduction was observed for IS and TCRpMHCmodels, especially for TCR and CDR predictions. In this context, AF2 outperforms IS and TCRpMHCmodels in the modeling of TCRs and CDRs, while presenting slightly higher averages than TCRmodel2. However, AF2's poor performance for the "all protein" group persisted, and was driven by inaccurate predictions of the docking orientation of the TCR. This issue is also reflected in the impaired performance of TCRmodel2 in this "all protein" group (e.g., note the high standard deviation in Fig. 5(a)). Interestingly, the docking-based method used by IS produced the lowest RMSD average and the lowest standard deviation.

In order to better characterize the contribution of inaccurate TCR docking orientation to our "all protein" RMSD results, we conducted a series of additional evaluations using (i) the CAPRI assessment [34], (ii) the DockQ score [41], and (iii) the measurement of the TCR angles with TCR3d [36]. Across the entire dataset, the "high" CAPRI accuracy fraction of AF2 models stands at approximately 5%, which is significantly lower than all other methods, for which it can reach around 50-65% (Fig. 6(a)). Additionally, the "incorrect" fraction of AF2 models is the highest of the three, approaching 40%. Notably, TCRmodel2 was the method with the largest fraction of models within the "high" accuracy category, but it also had two models within the lower "acceptable" CAPRI accuracy, namely 1AO7 and 7N1E. IS and TCRpMHCmodels had similar fractions of models within the high and medium categories and had no models classified as acceptable or incorrect.

Furthermore, in the new dataset, for which all the structures are not included in the training sets of these web servers, we observed that TCRmodel2 still performed well, with approximately 60% of models achieving high CAPRI accuracy, while IS and TCRpMHCmodels failed to produce any models of this level. Nevertheless, all models from these two methods maintained a "medium" CAPRI classification. This outcome is in line with the high variation in RMSD and DockQ scores, where we noticed a higher standard deviation for TCRmodel2 as compared to IS and TCRpMHCmodels (Fig. 5, 6(b)).

We then conducted another analysis to evaluate the predictive accuracy of methodologies in determining the crossing angle and incident angle of the modeled TCRs. Our findings are consistent with prior research [28] showing that AF2 lags behind other methods in aligning docked complexes, including TCRs to pMHCs [42]. Furthermore, we observed no significant disparity between the IS, TCRmodel2, and TCRpMHCmodels in this context (Fig. 6(c), 6(d)).

3.3. Higher prediction consistency can prevent high accuracy prediction

After recognizing that inaccuracies in TCR docking orientation can be very detrimental to AF2-based predictions, we decided to test how much improvement over the baseline AF2 predictions could be achieved by simply improving the docking orientation of TCRpMHC models. For that, we implemented a hybrid protocol combining AF2 and IS methods (Fig. 4) and repeated all analyses to compare the models produced by this hybrid approach with those produced by the other methods. Interestingly, even this simplistic hybrid implementation outperformed AF2, IS, and TCRpMHCmodels, producing Cα RMSD averages that approximate those of TCRmodel2 (Fig. 7). The hybrid method presented

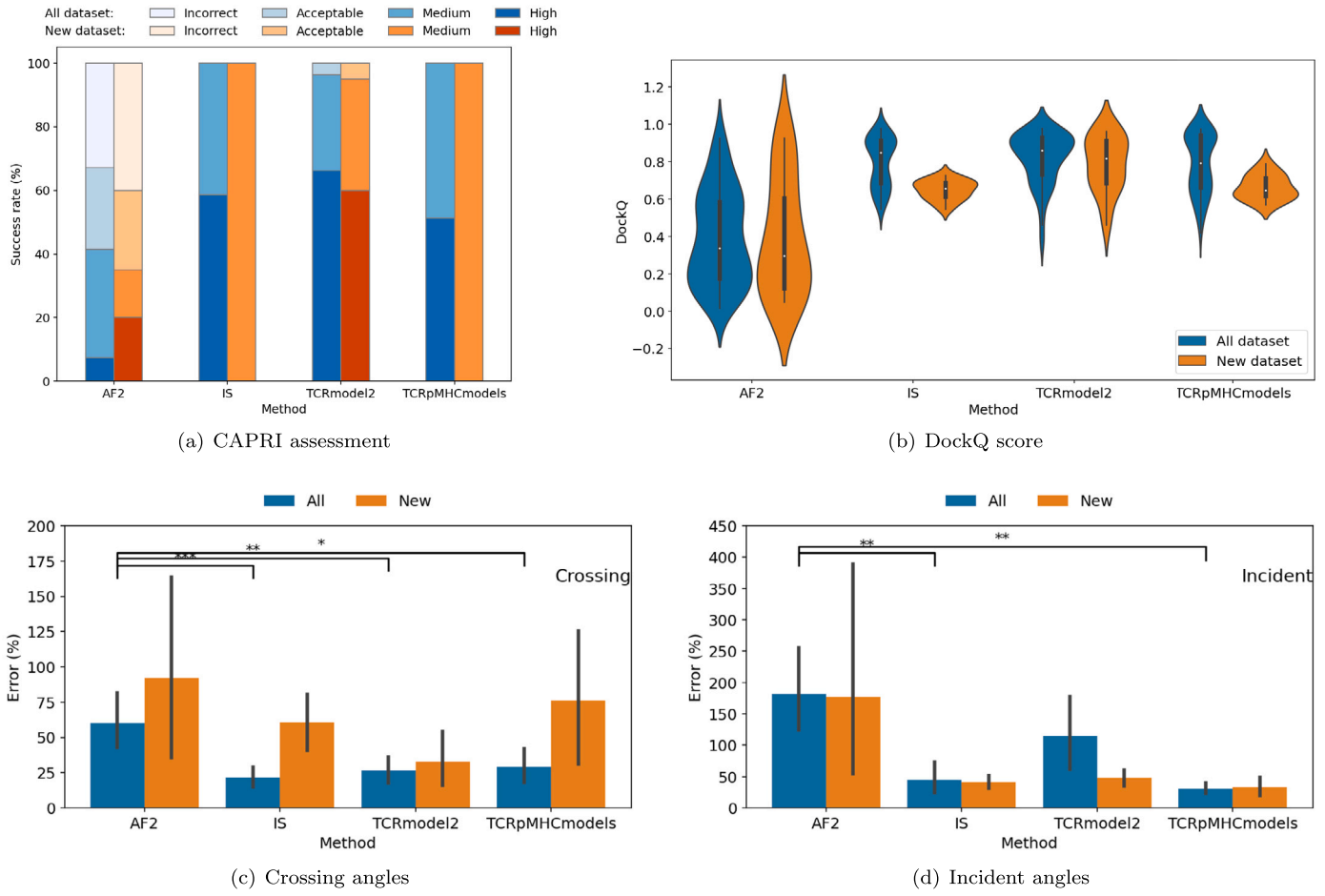

(a) CAPRI assessment (b) DockQ score

(c) Crossing angles (d) Incident angles

Fig. 6. Model accuracy according to (a) CAPRI assessment, (b) DockQ score, (c) Crossing angle, and (d) Incident angle. Independent models were produced using four different methods (AF2, IS, TCRmodel2, and TCRpMHC). These analyses were conducted for a set of 87 TCRpMHC structures ("All dataset"), or a subset of 20 structures published after 2021 ("New dataset").

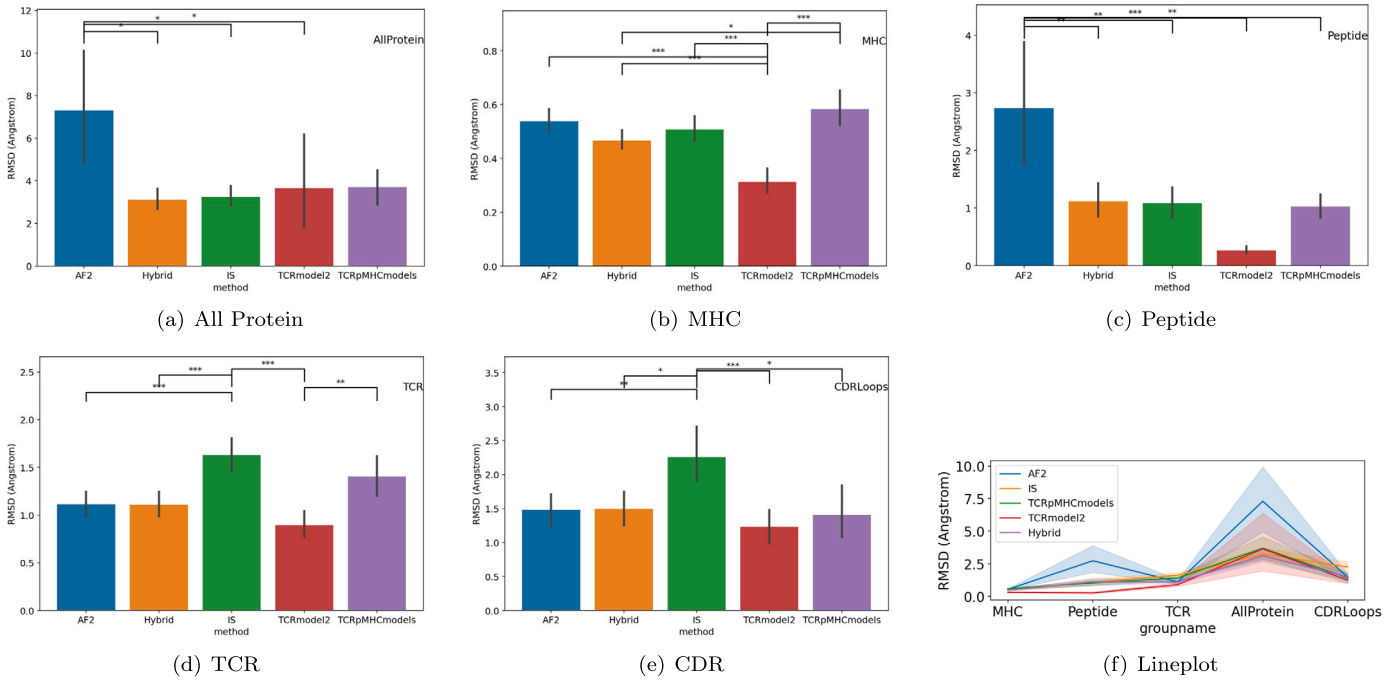

(a) All Protein (b) MHC (c) Peptide

(d) TCR (e) CDR (f) Lineplot

Fig. 7. Carbon alpha root mean square deviation (Cα RMSD) of a subset of 20 structures published after 2021 ("new dataset") modeled from different methods: AF2, IS, TCRpMHCmodels, TCRmodel2 and hybrid compared to crystal structures. The average RMSD was measured from different groups of atoms: (a) all protein, (b) MHC, (c) peptide, (d) TCR chains, (e) CDR loops, and (f) line plots showing the variation in predicting different groups of all methods.

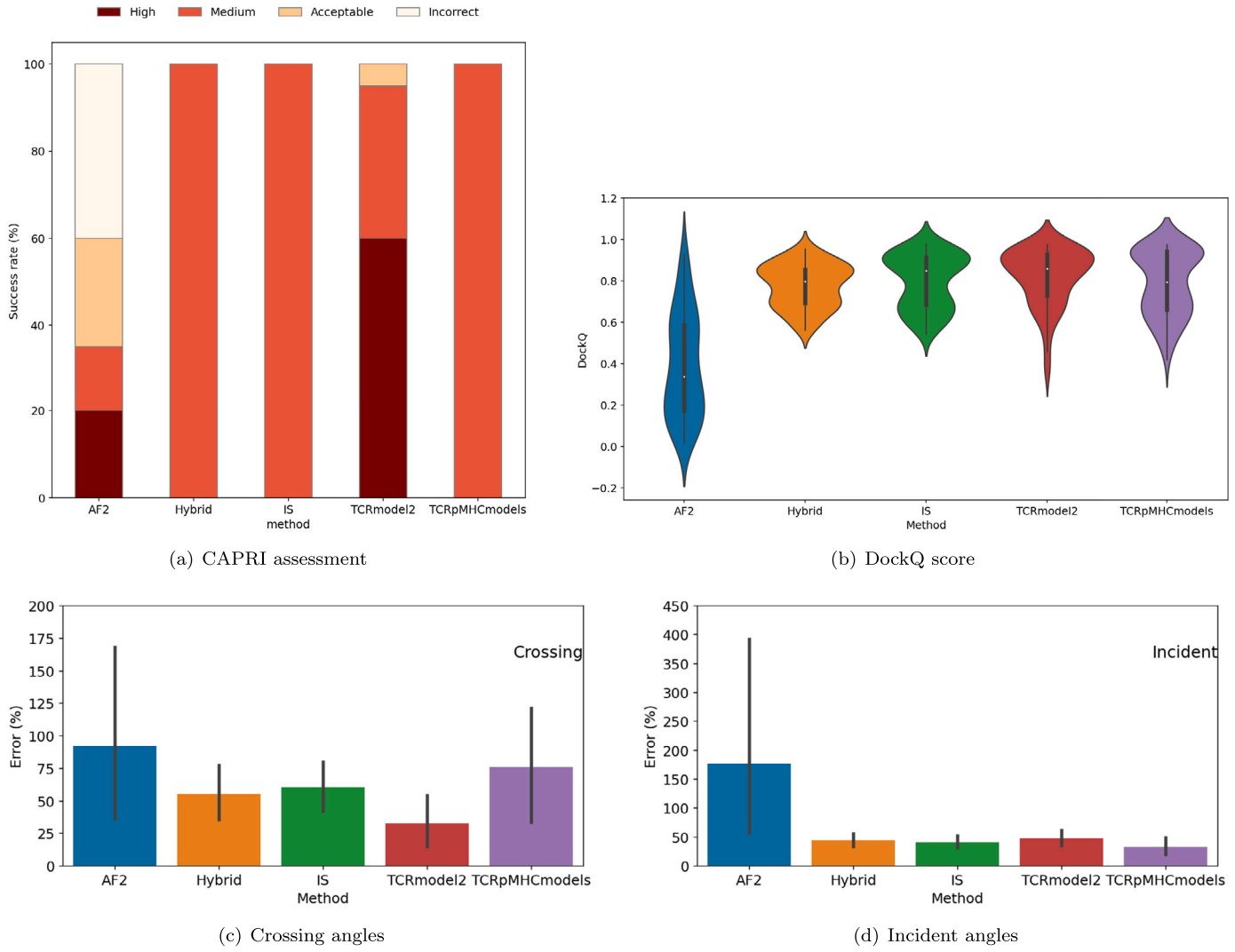

(a) CAPRI assessment

(b) DockQ score

(c) Crossing angles

(d) Incident angles

Fig. 8. Docking orientation assessment of a subset of 20 structures published after 2021 ("new dataset") modeled with 5 different methods: AF2, IS, TCRmodel2, TCRpMHC, and hybrid approach. (a) CAPRI assessment, (b)DockQ score, (c) crossing angles, and (d) incident angles.

a lower average and standard deviation than TCRmodel2 for the "all protein" group, demonstrating there is room for improvement in AF2-based methods with regards to the TCR docking orientation [43]. There was also no significant difference between hybrid/AF2 and TCRmodel2 on the prediction of CDR loops. Regardless, the RMSD results show TCRmodel2 is still significantly better than this hybrid approach when predicting the TCR, the MHC, and, most remarkably, the peptide conformations (Fig. 7(c)).

Next, all hybrid models were subject to evaluation using CAPRI, DockQ, and TCR angles to compare their performance against other methods. Leveraging IS's docking-based method, the hybrid models exhibited better results in DockQ scores and TCR angles than AF2. Within the CAPRI framework, the hybrid models consistently demonstrated "medium" performance levels across all models, resulting in a low standard deviation in RMSD and DockQ (Fig. 7-8). However, this increased consistency came with the cost of not producing models within the "high" accuracy category, which were obtained with AF2 and TCRmodel2. The improved performance of TCRmodel2 in the CAPRI assessment, as compared to the hybrid approach, highlight additional benefits of the customized protocol, going beyond the improvement in TCR docking orientation in relation to AF2.

Finally, we utilized a variance graph to gain deeper insights into the diversity of TCR docking orientations across TCRpMHC complexes (Fig. 9). Upon assessing the TCR crossing and incident angles for our selection of crystal structures (All Dataset), we noted a significant diversity of TCR orientations. This happens in spite of a higher prevalence of HLA-A2 MHCs in our dataset (i.e., limited diversity of MHC restrictions) and the potential packing effects of the X-ray crystallography protocols. When comparing the variance of experimentally determined structures with that of the corresponding models, we see clear differences between the modeling methods. On one hand, the deep-learning approach of AF2 and TCRmodel2 produced much higher variance of incident angles when compared to crystals and "template-based" models (i.e., based on docking or homology modeling). This higher variance reflects greater flexibility of the modeling protocol, therefore allowing for the accurate prediction of less common TCR orientations. However, such flexibility comes with the cost of greater inconsistency of predictions, and the potential to produce models that are very far from the reference crystal structure. On the other hand, IS and TCRpMHCmodels produce much more consistent predictions for incident angles, with a variance that is lower than that of the crystal structures. Unfortunately, this reflects a more rigid modeling protocol, which can often be unable to reproduce the TCR docking orientation with high accuracy. Another interesting finding is that the variance of incident angles is independent of the variance of crossing angles. For instance, IS and the Hybrid approaches show a pattern of crossing/incident variance that is more similar to that of crystal structures, with somewhat higher variance for crossing angles. AF2 models also show higher variance of crossing angles compared with

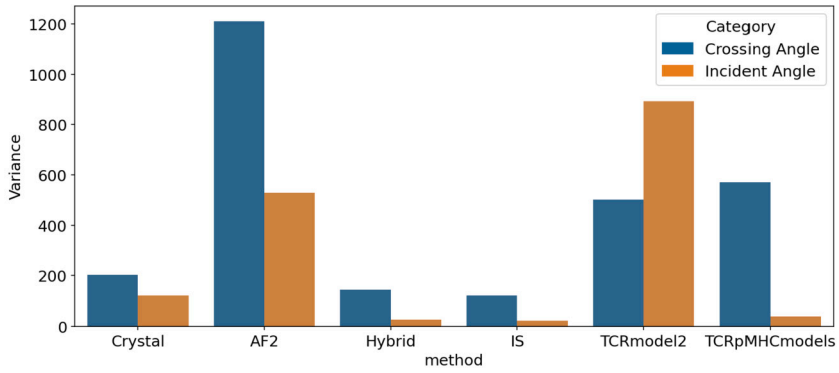

Fig. 9. Variance of TCR docking angles in all models produced by different methods, including AF2, IS, TCRmodel2, TCRpMHCmodels and hybrid, and their corresponding crystal structures, computed across 87 TCRpMHC structures ("all dataset").

incident angles, but both at a level much higher than crystals, Hybrid, and IS models. Variance is also high for TCRmodel2 predictions, but the pattern is reversed. The customized implementation of TCRmodel2 reduced the variance of crossing angles to less than half of that calculated for AF2, but produced the highest variance of incident angles across all analyses. Finally, TCRpMHCmodels produced intermediate results, with crossing angle variance equivalent to TCRmodel2, and incident angle variance almost as low as that of IS and the Hybrid method.

4. Conclusion

The accurate and scalable structural modeling of TCRpMHC complexes remains an open problem in immunoinformatics and computational oncology [27,44]. Although multiple methods have been proposed for predicting the structures of pMHCs [38,45,40] and TCRs [2,29], resolving the TCRpMHC complex brings additional challenges, particularly regarding the TCR orientation.

In recent years, there has been a growing demand for more accurate and efficient methods for the prediction of the 3D structures of TCRpMHC complexes, with particular interest in TCR engineering applications for cancer immunotherapy [27,44]. To meet this growing need, web servers like TCRpMHCmodels and ImmuneScape were developed. These web servers use sophisticated algorithms and tailored computational approaches to process the amino acid sequences of the individual protein chains and to predict the 3D structures of the full TCRpMHC complexes.

In parallel to these efforts tailored for immunology applications, a modeling revolution has been enabled by the combined use of multiple sequence alignment (MSA) data and advanced deep learning methods [46]. Compared to other methods, AlphaFold2 [28] has shown remarkable accuracy in predicting individual protein structures but has struggled to model some macromolecular complexes, particularly TCRpMHC structures. By incorporating target-specific customization, AF2-based methodologies can significantly improve the prediction of protein complexes [47]. This development has paved the way for the creation of several other approaches using AF2 for customized applications, including TCRmodel2 [2]. Overall, these recent developments have brought about a significant shift in the field of TCRpMHC complex prediction. With the help of these new tools and approaches, higher confidence prediction of TCRpMHC structures is becoming possible, although the current computational efficiency of AF-based methods might still represent a limiting factor for large-scale modeling.

Here, we evaluated the performance of these four alternative methods using a curated dataset of 87 experimentally determined structures of TCRpMHC complexes. Since some of these complexes were used to develop the modeling methods, we further evaluated the methods in a subset of 20 structures published after 2021. Our analysis indicates that one of the major challenges in modeling TCRpMHC complexes is the high flexibility of the docking orientation between the TCR and pMHC. The TCR is known to have a preferred docking orientation (or "footprint"), with the TCRα chain mostly positioned on top of the MHC-I α2 domain and the TCRβ chain mostly situated above the α1 domain, in a preferred crossing angle [48,43,1]. However, an increasing diversity of TCR docking orientations is been reported as more structures are resolved with experimental methods, including the occurrence of a completely reversed orientation [23,4]. Naturally, this greater diversity of possible docking orientations represents an even greater challenge for modeling methods.

In spite of the incredible diversity of TCRpMHC structures, both in terms of amino acid sequences and docking orientations, our results show that good approximations can usually be obtained with very efficient methods such as TCRpMHCmodels and IS, and even better results can be obtained with newer deep-learning approaches such as TCRmodel2, although with lower computational efficiency and greater variance of results. This last point was further demonstrated by our implementation of a hybrid protocol combining the AF2 prediction of TCRs with the IS prediction of pMHCs and docking orientations. On one hand, these hybrid predictions were more consistent than those of TCRmodel2, preventing the generation of models that were further away from the corresponding crystal structures (e.g., acceptable models on the CAPRI assessment). Therefore, efforts to improve the TCR docking orientation, either as part of the modeling protocols or as additional refinement steps, have the greatest potential to advance our overall capacity to accurately predict the structures of TCRpMHC complexes [49,50]. On the other hand, this cannot be achieved by simply imposing additional constraints to limit the diversity of predicted crossing/incident angles, since this will come with the cost of not reproducing most complexes with the highest possible accuracy.

Note that our analysis is naturally limited by the dataset used to evaluate the different methods. Experimentally determined structures of TCRpMHC complexes are still mostly limited to X-ray crystallography studies, and available structural datasets are still small and biased, especially when considering only human class I MHCs. Our "All dataset" includes a diversity of peptide sequences but reflects the aforementioned bias with regards to the prevalence of HLA-A*02 alleles. As expected, limited diversity became an even bigger problem when considering the "New dataset", in which we were limited to the analysis of structures made available after 2021. Despite these limitations our analysis provides clear insights into the differences between the methods, the high level of accuracy that is already available in terms of CDR and peptide prediction, and the remaining challenges regarding the accurate prediction of TCR orientations. Future efforts to validate TCRpMHC modeling methods should leverage larger and more diverse datasets, potentially including class II MHCs, which should also be enabled by the increasing use of cryogenic electron microscopy (Cryo-EM) [51] to resolve TCRpMHC complexes.

Finally, it is also important to note that the activation of $CD8^+$ T cells is not entirely determined by the structural features of the TCRpMHC

complexes, but is also dependent on (i) several co-stimulatory signals mediated by essential molecules such as CD28, CD80, and CD86, and (ii) the influence of various cytokines, including IL-2 and IFN-γ [52]. Therefore, future development of novel and improved T-cell-based immunotherapy approaches depends on both (i) the continued advancement of computational methods for the modeling of TCRpMHC complexes, potentially including more biophysically accurate refinement protocols to account for the dynamics and flexibility of TCRpMHC interactions, and (ii) a broader understanding of the intricate interplay of other molecular signals driving $CD8^+$ T cell activation, and its impacts driving target-specificity and off-target toxicity.

Funding

This work was supported in part by funds from the University of Houston.

CRediT authorship contribution statement

Hoa Nhu Le: Writing – original draft, Visualization, Validation, Software, Methodology, Formal analysis, Data curation. **Martiela Vaz de Freitas:** Writing – review & editing, Visualization, Software, Data curation, Conceptualization. **Dinler Amaral Antunes:** Writing – review & editing, Supervision, Resources, Project administration, Investigation, Funding acquisition, Conceptualization.

Declaration of competing interest

None declared.

Acknowledgement

This work used the Extreme Science and Engineering Discovery Environment, which is supported by National Science Foundation Grant No. ACI1548562; more specifically, the work involved the use of the Stampede cluster at the Texas Advanced Computing Center, funded through Allocation No. TG-BIO220107. This work was completed in part with resources provided by the Research Computing Data Core at the University of Houston. We thank Finn Beruldsen for valuable comments on the final manuscript.

References

[1] Antunes DA, Rigo MM, Freitas MV, Mendes MFA, Sinigaglia M, Lizée G, et al. Interpreting T-cell cross-reactivity through structure: implications for TCR-based cancer immunotherapy. Front Immunol 2017;8:1210.
[2] Yin R, Ribeiro-Filho HV, Lin V, Gowthaman R, Cheung M, Pierce BG. TCRmodel2: high-resolution modeling of T cell receptor recognition using deep learning. Nucleic Acids Res 2023:gkad356.
[3] Antunes DA, Abella JR, Devaurs D, Rigo MM, Kavraki LE. Structure-based methods for binding mode and binding affinity prediction for peptide-MHC complexes. Curr Top Med Chem 2018;18(26):2239–55.
[4] Szeto C, Lobos CA, Nguyen AT, Gras S. TCR recognition of peptide–MHC-I: rule makers and breakers. Int J Mol Sci 2020;22(1):68.
[5] Zhang H, Lund O, Nielsen M. The pickpocket method for predicting binding specificities for receptors based on receptor pocket similarities: application to mhc-peptide binding. Bioinformatics 2009;25(10):1293–9.
[6] Morris GP, Allen PM. How the TCR balances sensitivity and specificity for the recognition of self and pathogens. Nat Immunol 2012;13(2):121–8.
[7] Rudolph MG, Wilson IA. The specificity of TCR/pMHC interaction. Curr Opin Immunol 2002;14(1):52–65.
[8] Attaf M, Legut M, Cole DK, Sewell AK. The T cell antigen receptor: the Swiss army knife of the immune system. Clin Exp Immunol 2015;181(1):1–18.
[9] Degauque N, Brouard S, Soulillou JP. Cross-reactivity of TCR repertoire: current concepts, challenges, and implication for allotransplantation. Front Immunol 2016;7:89.
[10] Sewell AK. Why must T cells be cross-reactive? Nat Rev Immunol 2012;12(9):669–77.
[11] Birnbaum ME, Mendoza JL, Sethi DK, Dong S, Glanville J, Dobbins J, et al. Deconstructing the peptide-MHC specificity of T cell recognition. Cell 2014;157(5):1073–87.
[12] Welsh RM, Che JW, Brehm MA, Selin LK. Heterologous immunity between viruses. Immunol Rev 2010;235(1):244–66.
[13] Fonseca AF, Antunes DA. CrossDome: an interactive R package to predict cross-reactivity risk using immunopeptidomics databases. Front Immunol 2023;14:1142573.
[14] Yang X, Nishimiya D, chte S, Jude KM, Borowska M, Savvides CS, et al. Facile repurposing of peptide-MHC-restricted antibodies for cancer immunotherapy. Nat Biotechnol 2023;41(7):932–43.
[15] Wang T, Navenot JM, Rafail S, Kurtis C, Carroll M, Van Kerckhoven M, et al. Identifying MAGE-A4-positive tumors for TCR T cell therapies in HLA-A*02-eligible patients. Mol Ther Methods Clin Dev 2024;32(2):101265.
[16] Lee SW, Lee HM. Engineered T cell receptor for cancer immunotherapy. Biomol Ther (Seoul) Jun 2024.
[17] Zou JL, Chen KX, Wang XJ, Lu ZC, Wu XH, Wu YD. Structure-based rational and general strategy for stabilizing single-chain T-cell receptors to enhance affinity. J Med Chem 2024;67(9):7635–46.
[18] Fodor J, Riley BT, Borg NA, Buckle AM. Previously hidden dynamics at the TCR-peptide-MHC interface revealed. J Immunol 2018;200(12):4134–45.
[19] Singh NK, Abualrous ET, Ayres CM, é F, Gowthaman R, Pierce BG, et al. Geometrical characterization of T cell receptor binding modes reveals class-specific binding to maximize access to antigen. Proteins 2020;88(3):503–13.
[20] Finnigan JP, Newman JH, Patskovsky Y, Patskovska L, Ishizuka AS, Lynn GM, et al. Structural basis for self-discrimination by neoantigen-specific TCRs. Nat Commun 2024;15(1):2140.
[21] Wang A, Lin X, Chau KN, Onuchic JN, Levine H, George JT. RACER-m leverages structural features for sparse T cell specificity prediction. Sci Adv 2024;10(20):eadl0161.
[22] McMaster B, Thorpe C, Ogg G, Deane CM, Koohy H. Can AlphaFold's breakthrough in protein structure help decode the fundamental principles of adaptive cellular immunity? Nat Methods 2024;21(5):766–76.
[23] Bradley P. Structure-based prediction of T cell receptor: peptide-MHC interactions. eLife 2023;12:e82813.
[24] Bank PD. Protein data bank. Nat, New Biol 1971;233(223):10–1038.
[25] Vita R, Overton JA, Greenbaum JA, Ponomarenko J, Clark JD, Cantrell JR, et al. The immune epitope database (IEDB) 3.0. Nucleic Acids Res 2015;43(D1):D405–12.
[26] Jensen KK, Rantos V, Jappe EC, Olsen TH, Jespersen MC, Jurtz V, et al. TCRpMHCmodels: structural modelling of TCR-pMHC class I complexes. Sci Rep 2019;9(1):14530.
[27] Li S, Wilamowski J, Teraguchi S, van Eerden FJ, Rozewicki J, Davila A, et al. Structural modeling of lymphocyte receptors and their antigens. In: Vitro differentiation of T-cells: methods and protocols; 2019. p. 207–29.
[28] Jumper J, Evans R, Pritzel A, Green T, Figurnov M, Ronneberger O, et al. Highly accurate protein structure prediction with AlphaFold. Nature 2021;596(7873):583–9.
[29] Klausen MS, Anderson MV, Jespersen MC, Nielsen M, Marcatili P. LYRA, a webserver for lymphocyte receptor structural modeling. Nucleic Acids Res 2015;43(W1):W349–55.
[30] Katoh K, Kuma K, Toh H, Miyata T. MAFFT version 5: improvement in accuracy of multiple sequence alignment. Nucleic Acids Res 2005;33(2):511–8.
[31] Krivov GG, Shapovalov MV, Dunbrack Jr RL. Improved prediction of protein side-chain conformations with SCWRL4. Proteins, Struct Funct Bioinform 2009;77(4):778–95.
[32] Yang Z, Zeng X, Zhao Y, Chen R. AlphaFold2 and its applications in the fields of biology and medicine. Signal Transduct Targeted Ther 2023;8(1):115.
[33] Shen M, Sali A. Statistical potential for assessment and prediction of protein structures. Protein Sci 2006;15(11):2507–24.
[34] Janin J, Henrick K, Moult J, Eyck LT, Sternberg MJ, Vajda S, et al. CAPRI: a critical assessment of predicted interactions. Proteins, Struct Funct Bioinform 2003;52(1):2–9.
[35] Lensink MF, Wodak SJ. Score_set: a CAPRI benchmark for scoring protein complexes. Proteins, Struct Funct Bioinform 2014;82(11):3163–9.
[36] Gowthaman R, Pierce BG. TCR3d: the T cell receptor structural repertoire database. Bioinformatics 2019;35(24):5323–5.
[37] SciPy tukey's hsd test, https://docs.scipy.org/doc/scipy/reference/generated/scipy.stats.tukey_hsd.html. [Accessed 22 May 2024].
[38] Fasoulis R, Rigo MM, Lizée G, Antunes DA, Kavraki LE. APE-Gen2.0: expanding rapid class I peptide-major histocompatibility complex modeling to post-translational modifications and noncanonical peptide geometries. J Chem Inf Model 2024;64(5):1730–50.
[39] McDonald EF, Jones T, Plate L, Meiler J, Gulsevin A. Benchmarking AlphaFold2 on peptide structure prediction. Structure 2023;31(1):111–9.
[40] Gupta S, Nerli S, Kutti Kandy S, Mersky GL, Sgourakis NG. HLA3DB: comprehensive annotation of peptide/HLA complexes enables blind structure prediction of T cell epitopes. Nat Commun 2023;14(1):6349.
[41] Basu S, Wallner B. DockQ: a quality measure for protein-protein docking models. PLoS ONE 2016;11(8):e0161879.
[42] Yin R, Feng BY, Varshney A, Pierce BG. Benchmarking AlphaFold for protein complex modeling reveals accuracy determinants. Protein Sci 2022;31(8):e4379.
[43] Peacock T, Chain B. Information-driven docking for TCR-pMHC complex prediction. Front Immunol 2021;12:686127.

[44] Borrman T, Pierce BG, Vreven T, Baker BM, Weng Z. High-throughput modeling and scoring of TCR-pMHC complexes to predict cross-reactive peptides. Bioinformatics 2020;36(22–23):5377–85.
[45] Marzella DF, Parizi FM, Tilborg Dv, Renaud N, Sybrandi D, Buzatu R, et al. PANDORA: a fast, anchor-restrained modelling protocol for peptide: MHC complexes. Front Immunol 2022;13:878762.
[46] Sapoval N, Aghazadeh A, Nute MG, Antunes DA, Balaji A, Baraniuk R, et al. Current progress and open challenges for applying deep learning across the biosciences. Nat Commun 2022;13(1):1728.
[47] Motmaen A, Dauparas J, Baek M, Abedi MH, Baker D, Bradley P. Peptide-binding specificity prediction using fine-tuned protein structure prediction networks. Proc Natl Acad Sci 2023;120(9):e2216697120.
[48] Adams JJ, Narayanan S, Liu B, Birnbaum ME, Kruse AC, Bowerman NA, et al. T cell receptor signaling is limited by docking geometry to peptide-major histocompatibility complex. Immunity 2011;35(5):681–93.
[49] Deng L, Ly C, Abdollahi S, Zhao Y, Prinz I, Bonn S. Performance comparison of TCR-pMHC prediction tools reveals a strong data dependency. Front Immunol 2023;14:1128326.
[50] Alba J, D'Abramo M. The full model of the pMHC-TCR-CD3 complex: a structural and dynamical characterization of bound and unbound states. Cells 2022;11(4):668.
[51] Saotome K, Dudgeon D, Colotti K, Moore MJ, Jones J, Zhou Y, et al. Structural analysis of cancer-relevant TCR-CD3 and peptide-MHC complexes by cryoEM. Nat Commun 2023;14(1):2401.
[52] Goronzy JJ, Weyand CM. T-cell co-stimulatory pathways in autoimmunity. Arthritis Res Ther 2008;10:1–10.